Supporting Information

Interplay of non-uniform charge distribution on the electrochemical modification of graphene

Lucyano J. A. Macedo[a], Filipe C. D. A. Lima[b], Rodrigo G. Amorim[c], Raul O. Freitas[d], Anur Yadav[e], Rodrigo M. Iost[e], Kannan Balasubramanian[e], and Frank N. Crespilho[a]*

[a]*São Carlos Institute of Chemistry, University of São Paulo, São Paulo 13560-970, Brazil. E-mail: frankcrespilho@iqsc.usp.br*

[b]*Federal Institute of Education, Science, and Technology of São Paulo, Campus Matão, São Paulo 15991-502, Brazil*

[c]*Department of Physics, ICEx, Fluminense Federal University, Volta Redonda, Rio de Janeiro 27213-145, Brazil*

[d]*Brazilian Synchrotron Light Laboratory (LNLS), Brazilian Center for Research in Energy and Materials (CNPEM), Campinas, São Paulo 13083-970, Brazil*

[e]*Department of Chemistry, School of Analytical Sciences Adlershof (SALSA) and IRIS Adlershof, Humboldt-Universität zu Berlin, Berlin 10099, Germany*

*e-mail: frankcrespilho@iqsc.usp.br

Contents

A. Removal of copper residues from graphene

Copper residues from the support used in the chemical vapor deposition are typically left over on graphene, even after etching with an oxidizing solution of HCl and H_2O_2 (1.4 and 0.5 mol·L^{-1}, respectively). To ensure complete removal of such metal residues, an electrochemical etching (e-etching) procedure was carried out. Here, the electrode underwent potential cycling in HCl (0.1 mol·L^{-1}) until the signal from contamination completely disappears, as shown in Figure S1. After this treatment, the electrode is mainly composed of graphene only.

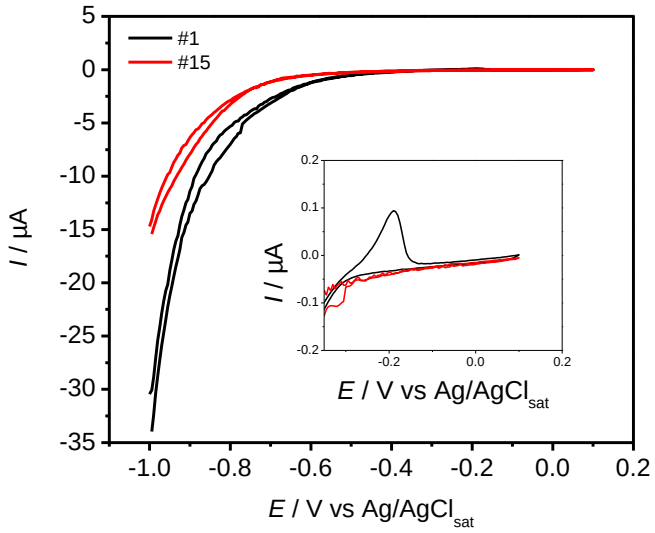

Figure S1. Removal of the residual copper from graphene. Cyclic voltammograms (CVs) show the disappearance of copper oxidation signals. Inset: A close-up view of the CV showing the disappearance of the oxidation signal.

B. Raman spectroscopy

We used Lorentzian function to fit the peaks of the Raman spectra of the graphene electrodes (Figure S2) and estimate the defect density after the functionalization calculate using the intensity ratio (I_D/I_G). After obtaining these ratio values, we applied the approach reported by Lucchese and co-workers [S1].

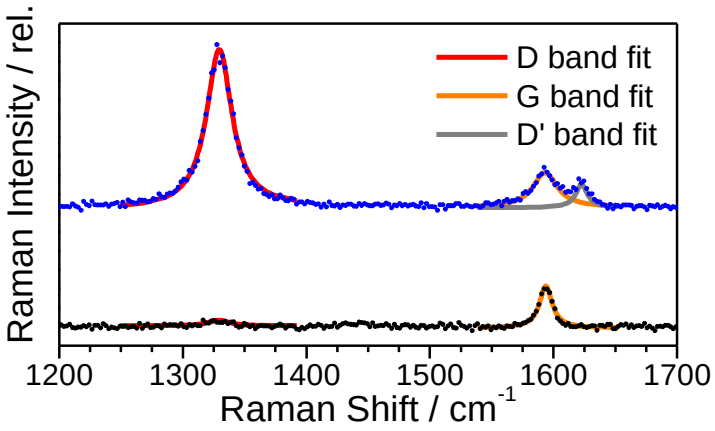

Figure S2. Raman spectra of (●) pristine and (●) functionalized graphene electrodes with the fits of each band highlighted as continuous lines.

Table S1 - Integrated intensity for each peak in the Raman spectra and their ratio for calculating the defect density

Graphene sample	I_D	I_G	I_D/I_G
Pristine	4.99	21.6	0.23
4-CP-functionalized	165	34.7	4.76

There are three stages of classification of disorder to analyze the Raman data of carbon materials along the amorphization trajectory: graphite to tetrahedral amorphous carbon. For graphene, stage 1 and stage 2 are most relevant.

Stage 1, in the Raman spectrum (a) D appears and I_D/I_G increases; (b) D′ appears; (c) all peaks broaden. (d) D + D′ appears.

In stage 2, (a) the G peak position down-shifts from ~1600 cm^{-1} toward ~1510 cm^{-1}; (b) I_D/I_G decreases toward 0, and (c) there are no more well-defined second-order peaks, but a broad feature from ~2300 to ~3200 cm^{-1} modulated by the 2D, D + D′, and 2D′ bands.

Using a 633 nm (1.96 eV) excitation laser, the parameters used in the equation S1 are $C_A = 10$; $C_S = 0.86$; $r_a = 3$; $r_s = 1$, which provides the plot presented in Figure S3.

$$\frac{I_D}{I_G} = C_A \cdot \frac{r_a^2 - r_s^2}{r_a^2 - 2r_s^2}\left[\exp\left(\frac{-\pi \cdot r_s^2}{L_D^2}\right) - \exp\left(\frac{-\pi(r_a^2 - r_s^2)}{L_D^2}\right)\right] + C_S \cdot \left[1 - \exp\left(\frac{-\pi \cdot r_s^2}{L_D^2}\right)\right] \quad \text{(S1)}$$

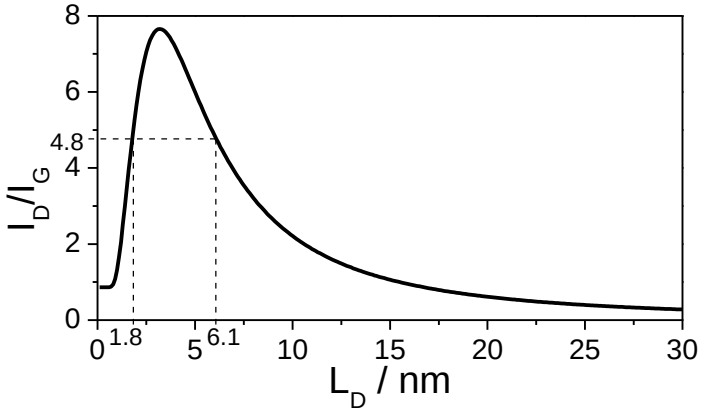

Figure S3. Fitted I_D/I_G as function of the average distance between the defects (L_D), in close concord to the data reported in reference S2.

For each I_D/I_G value (in our case it is 4.8), two L_D values will be obtained, one in each stage, where left side of the peak is the second stage and right side is the first stage. For I_D/I_G = 4.8, we get two L_D values: 1.8 nm and 6.1 nm.

The Raman spectrum in our case is in the first stage since D peak appears and I_D/I_G increases; D′ appears; after functionalization. Also, all the peaks broadened slightly and still we can see the sharp second order features in Raman spectrum. There is no change in G peak position: ~1593 cm^{-1}. Therefore, L_D will be around 6 nm.

This can also be confirmed by using the relation between FWHM(D) Γ_D, FWHM(G) Γ_G and L_D. Our values of Γ_D = 23.4 and Γ_G = 18.8 are consistent with those Ref. S2 (Figure 5), if we take L_D as ~5 nm.

Defect density can be calculated by the following equation,

$$n_D(cm^{-2}) = \frac{10^{14}}{\pi L_D^2}$$

When L_D = 6.1 nm, $n_D = 8.84 \times 10^{11}$ cm^{-2}.

C. Nano-FTIR of graphene sheet

Using the instrumentation of nano-FTIR/s-SNOM in the facilities of the Brazilian Synchrotron Light Laboratory (LNLS) we first analyzed a 4-CP-functionalized graphene sheet through nano-FTIR and observed no peaks related to either C=O or C=C as observed by micro-FTIR. On the other hand, a characteristic peak of Si-O stretching mode is observed, from the substrate where the graphene is supported on.

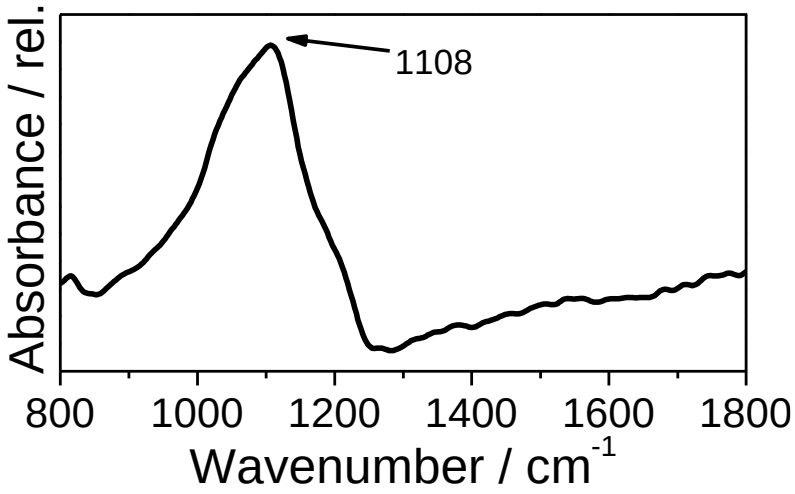

Figure S4. Nano-FTIR of 4-CP-functionalized graphene. Spectrum shows only a strong absorption of the Si-O stretching mode from the substrate underneath the graphene sheet.

D. Other samples AFM/s-SNOM data

Some other samples were analyzed through s-SNOM and the topographic profile and optical response confirms the concentration of functionalization on the edges of the graphene sheet.

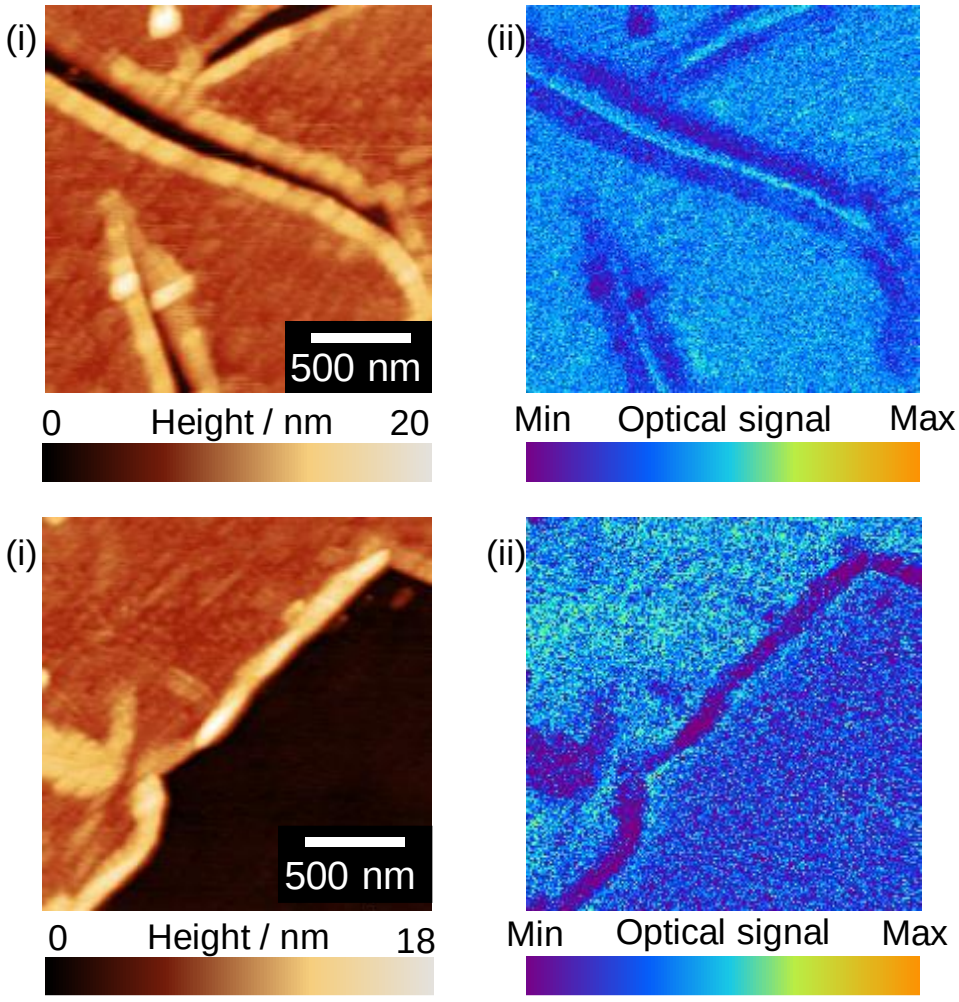

Figure S5. AFM and s-SNOM of 4-CP-functionalized graphene. i) Topographic images of the boundary between the graphene sheet and the SiO_2 substrate; ii) Simultaneous s-SNOM image of the optical response to broadband IR radiation.

We also analyzed the change in the topographic profile of the same region in a graphene electrode, by AFM imaging before and after the functionalization procedure. Similar results were obtained as discussed in Figure 2a,d.

The images were obtained using a commercial Dimension IV AFM working in tapping mode.

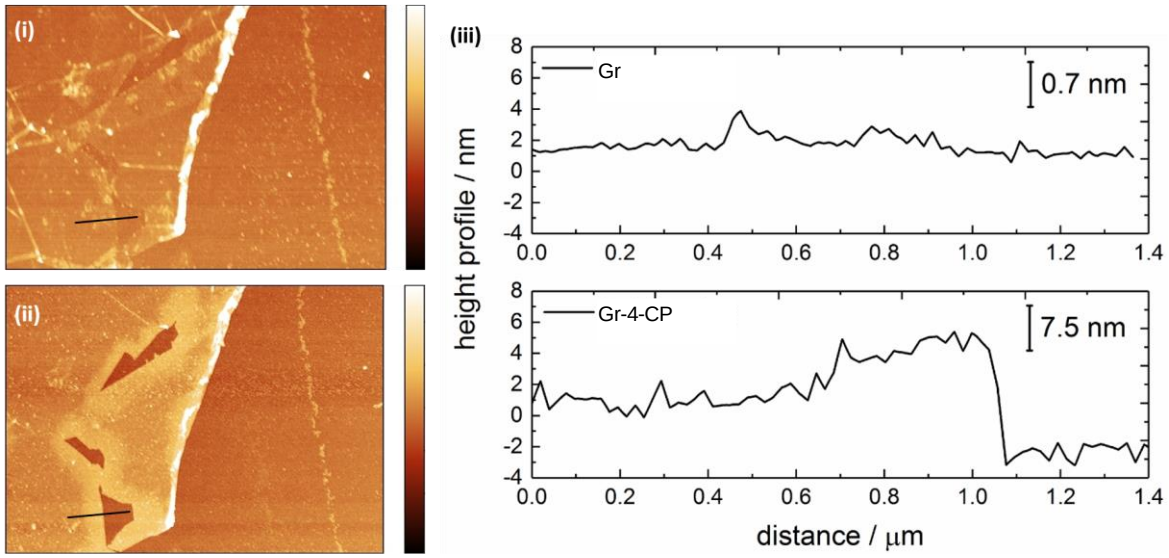

Figure S6. AFM images of the same region of the electrode (i) before and (ii) after the electrochemical attachment of 4-CP units. (iii) Height profiles along the black lines before (Gr, shown in (i)) and after (Gr-4-CP, shown in (ii)) the modification.

E. Additional Simulation Results

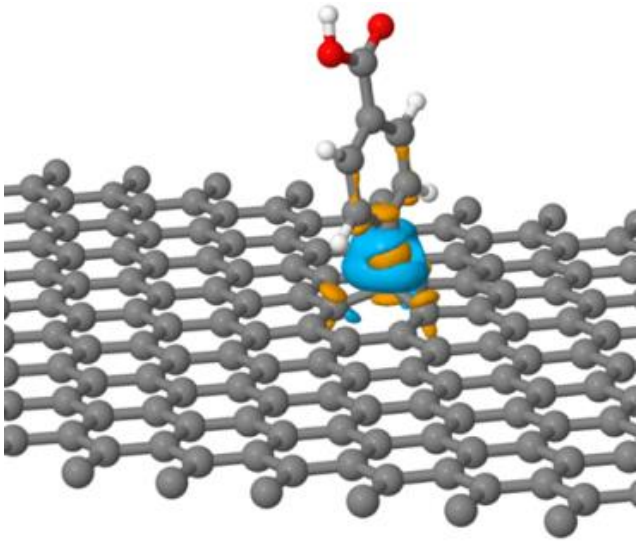

Figure S7. Local electronic density difference after functionalizing graphene. Charge difference of a system composed of a graphene sheet with 4-CP groups covalently anchored, showing the charges cluster on the sp3-hybridized carbon atom. Atom colors: C (gray), H (white), and O (red); orange and blue spheroids represent accumulations and depletions of electronic charge, respectively.

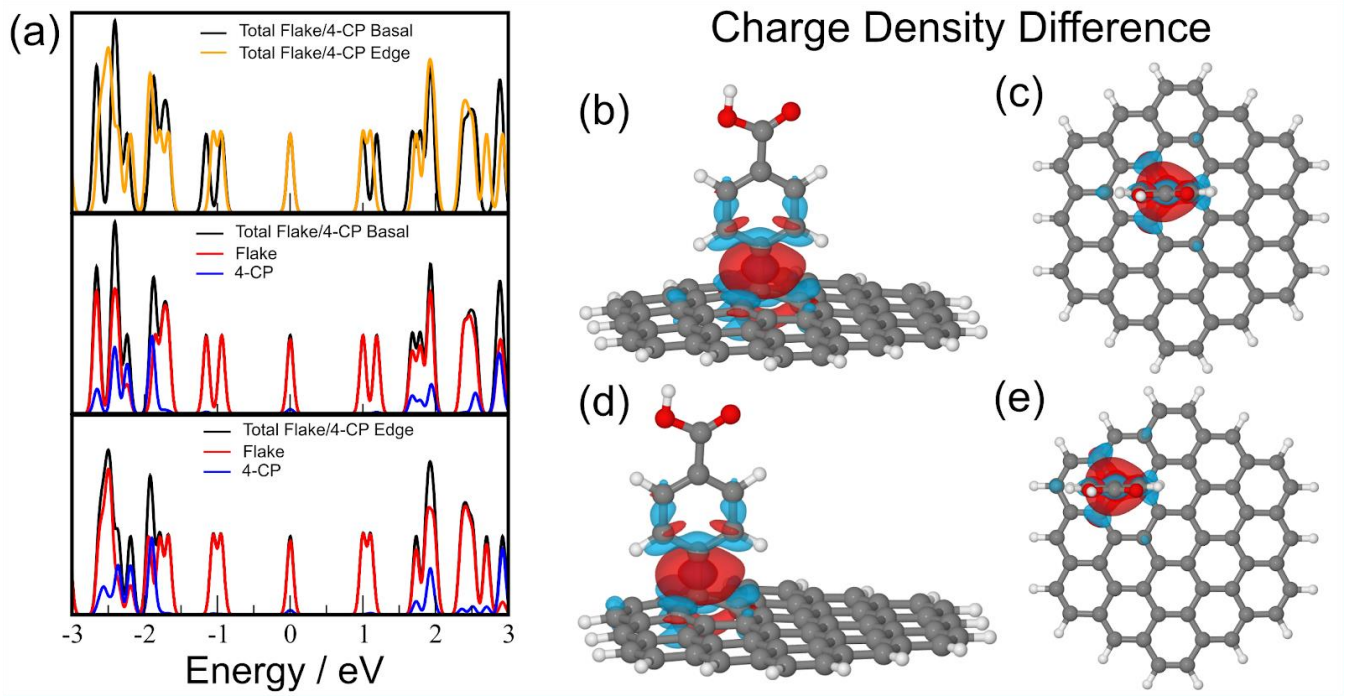

Figure S8. (a) PDOS for graphene nanoflakes functionalized with 4-CP. Local electronic density difference after functionalizing a graphene flake (b,c) basal region and (d,e) near the edges. Atom colors: C (gray), H (white), and O (red); orange and blue spheroids represent accumulations and depletions of electronic charge, respectively.

Figure S7 shows the charge density difference ($\rho_{diff} = \rho_{GR/4-CP} - (\rho_{GR} + \rho_{4-CP})$) for 4-CP adsorbed on graphene. This quantity estimates how the charge is redistributed through the investigated system. We note that the charge is localized in the GR/4-CP covalent bond and in its neighborhood. Furthermore, there is negligible charge concentrated in the carboxylic acid group.

Figure S8a shows the Projected Density of States (PDOS) of two similar nanoflakes composed by 86 atoms. The border dangling bonds were saturated with hydrogen atoms to avoid spurious states. The total DOS is shown in upper panel of Figure S8a, where two nanoflakes with 4-CP were compared at the basal and edge region. The central peaks are similar at the HOMO-1 and LUMO+1 with a small difference. The results for the central peak are very similar in comparison with GR/4-CP as well as the graphene ribbon. Figure S8a (central panel) shows the contribution of flake and 4-CP, where there are hybridization states between the flake and the 4-CP states at Fermi level. Moreover, the states from 4-CP appear for energies lesser than 2.0 eV or bigger than 2.0 eV. For 4-CP near the edge, the result is very similar to the basal one. The LUMO+1 has bigger intensity compared to the previous and it is a state that split in three small ones. The charge density differences are shown for the flakes. Figure S8b,c for basal and d,e for edge 4-CP position. We note that the charge redistribution follows the GR previous results; however, for the edge case there is a charge located in the border region due to 4-CP proximity.

F. References

[S1] Lucchese, M. M.; Stavale, F.; Ferreira, E. H. M.; Vilani, C.; Moutinho, M. V. O.; Capaz, R. B.; Achete, C. A.; Jorio, A. *Carbon* **2010**, 48, 1592–1597.

[S2] Cançado, L. G.; Jorio, A.; Ferreira, E. H.; Stavale, F.; Achete, C. A.; Capaz, R. B.; Moutinho, M. V.; Lombardo, A.; Kulmala, T. S.; Ferrari, A. C. *Nano Lett.* **2011**, 11, 3190-3196.